Imaging Physicochemical Reactions Occurring at the Pore Surface in Binary Bioactive Glass Foams by Micro Ion Beam Analysis

E. Jallot,*,† J. Lao,† Ł. John,†,‡,§,∥ J. Soulié,†,‡,§ Ph. Moretto,⊥,# and J. M. Nedelec‡,§

Clermont Université, Université Blaise Pascal, CNRS/IN2P3, Laboratoire de Physique Corpusculaire, BP 10448, F-63000 Clermont-Ferrand, France, Clermont Université, ENSCCF, Laboratoire des Matériaux Inorganiques, BP 10448, F-63000 Clermont-Ferrand, France, CNRS UMR 6002, LMI, F-63177 Aubière, France, Faculty of Chemistry, University of Wrocław, 14 F. Joliot-Curie, 50-383 Wrocław, Poland, Université de Bordeaux, Centre d'Etudes Nucléaires Bordeaux-Gradignan, UMR 5797, Gradignan F-33175, France, and CNRS/IN2P3, Centre d'Etudes Nucléaires Bordeaux-Gradignan, UMR 5797, Chemin du Solarium, BP 120, F-33175 Gradignan cedex, France

ABSTRACT In this work, the physicochemical reactions occurring at the surface of bioactive sol−gel derived 3D glass scaffolds via a complete PIXE characterization were studied. 3D glass foams in the SiO_2−CaO system were prepared by sol−gel route. Samples of glass scaffolds were soaked in biological fluids for periods up to 2 days. The surface changes were characterized using particle induced X-ray emission (PIXE) associated to Rutherford backscattering spectroscopy (RBS), which are efficient methods to perform quantitative chemical maps. Elemental maps of major and trace elements at the glass/biological fluids interface were obtained at the micrometer scale for every interaction time. Results revealed interconnected macropores and physicochemical reactions occurring at the surface of pores. The micro-PIXE-RBS characterization of the pores/biological fluids interface shows the glass dissolution and the rapid formation of a Ca rich layer with the presence of phosphorus that came from biological fluids. After 2 days, a calcium phosphate-rich layer containing magnesium is formed at the surface of the glass scaffolds. We demonstrate that quantities of phosphorus provided only by the biological medium have a significant impact on the development and the formation of the phosphocalcic layer.

KEYWORDS: PIXE-RBS methods • biomaterials • bioactive glass • sol−gel

1. INTRODUCTION

Clinical operations on bone defects and fractures may call for a filling material that also presents the ability to contribute to the healing process. Bioactive glasses are attractive biomaterials for filling bony defects, repairing damaged bony tissues, and struggling against troubles caused by osteoporosis (1). In contact with body fluids, bioactive glasses induce a complex series of physicochemical reactions leading to the formation of an interfacial bone-like apatite layer (2). This layer provides an ideal environment for bone cells proliferation and differentiation: new bone is formed that has a mechanically strong bond to the bioactive glass surface (3). The bioactivity mechanisms and growth of this apatite-like layer at the interface deeply depend on the composition and porosity of the glass. Thus determining parameters such as the material chemical composition and textural properties must be so chosen that the material might be used as an efficient implant, capable of forming a strong interfacial bond with host tissues and stimulating bone-cell proliferation (4, 5). Moreover, ionic dissolution products released from bioactive glasses during physicochemical reactions play an important role on cells behavior. It has been shown that these ionic dissolution products can promote regeneration of new tissue away from the glass surface, through the stimulation of cellular activity (6−8). For tissue-engineering applications, the ability of bioactive glasses to form an apatite layer and to release critical amounts of specific ions is of major interest.

For this purpose, a 3D glass scaffold in the SiO_2−CaO system has been developed for bone tissue engineering. Sol−gel derived bioactive glass foams have been prepared to obtain 3D bioactive scaffolds with hierarchical interconnected pores with morphologies similar to trabecular bone (9). This technique permits the synthesis of homogeneous materials with high porosity at low processing temperature (10). Another technique to produce porous scaffolds from bioactive glasses is based on the original melt-derived 45S5 composition (11). This way of synthesis permits to obtain scaffolds with enhanced mechanical properties. The scaffolds exhibit a hierarchical pore network with interconnected macropores higher than 400 μm, which is the minimum pore diameter required to guide the cell growth and to allow the synthesis of extracellular matrix in the human body. To better understand and to improve bioactive properties of the

* To whom correspondence should be addressed. Address: Laboratoire de Physique Corpusculaire de Clermont-Ferrand CNRS/IN2P3 UMR 6533, Université Blaise Pascal, 24 avenue des Landais, 63177 Aubière Cedex, France. Tel: 33 (0)4 73 40 72 65. Fax: 33 (0)4 73 26 45 98. E-mail: jallot@clermont.in2p3.fr.
Received for review March 17, 2010 and accepted May 25, 2010
† Clermont Université, Université Blaise Pascal.
‡ Clermont Université, ENSCCF.
§ CNRS UMR 6002.
∥ Faculty of Chemistry, University of Wrocław.
⊥ Université de Bordeaux, Centre d'Etudes Nucléaires Bordeaux-Gradignan.
CNRS/IN2P3, Centre d'Etudes Nucléaires Bordeaux-Gradignan.
DOI: 10.1021/am1002316

glass, it is essential to collect quantitative information regarding the physicochemical reactions occurring at the surface of the glass pores (12). Small volumes of gel−glass foams were immersed in biological fluids for varying periods. Interconnected macropores were expected to influence the in vitro bioactivity through physicochemical reactions at their surface. Analyses of major, minor, and trace elements present at the biomaterial/biological fluids interface were performed by particle-induced X-ray emission (PIXE) associated to Rutherford backscattering spectroscopy (RBS). Obtaining PIXE elemental maps at a micrometer scale permits the complete follow-up of the phosphocalcic layer formation along with major and trace element quantification. It allows important evaluation for the in vivo bioactivity of such a porous material.

2. MATERIALS AND METHODS

2.1. Preparation of the 3D Bioactive Glass Scaffolds. Gel−glass foams containing 75 wt % SiO_2−25 wt % CaO were prepared using the following procedure, based on the process first described by Jones et al. (4, 13−15): First, the sol preparation involved the delicate mixing of tetraethylorthosilicate (TEOS, $Si(OC_2H_5)_4$) in water and HCl mixture under ambient pressure. Then the required quantity of calcium nitrate ($Ca(NO_3)_2$, $4H_2O$) was added. On completion of hydrolysis (after 60 min stirring), 25 mL of sol were foamed by vigorous stirring with the addition of 0.5 mL of a surfactant (Teepol) and 0.75 mL of hydrofluoric acid as catalyst. The whole operation was conducted at 25 °C in a thermostatically controlled bath. About 15 min later, the viscosity sharply increased, and the gelling point was approached. The sol−gel foams were cast into airtight PTFE molds. Aging of the foams then occurred at 60 °C for 72 h, followed by drying at 130 °C for 48 h and a final thermal stabilization step at 700 °C for 24 h to achieve further densification. Finally, monolithic cylinders were obtained.

2.2. Materials Characterization. Apparent density of the samples was determined by measuring the dimensions (assuming cylindrical shape) of a sample of known mass. True density or skeleton density (without taking into account the pores volume) was measured by helium gas pycnometry with an Accupyc equipment (Micromeritics). Macroporosity was assessed by taking both optical and scanning electron microscopy images of the samples.

Nitrogen gas sorption analyses were performed to characterize the glasses mesoporosity. The samples were vacuum outgassed at 120 °C for 12 h to remove physically adsorbed molecules such as moisture from the pores. The adsorption/desorption isotherms were recorded on a Quantachrom Autosorb-1 apparatus. The instrument determined isotherms volumetrically by a discontinuous static method at 77 K. The surface areas were obtained by applying the BET method to the N_2 isotherm. The mesopore size distribution was determined by the BJH method on the desorption branch. Total mesoporous volume was measured at a relative pressure $P/P_0 = 0.995$.

Table 1. Ionic Concentrations of Inorganic Salts in SBF and DMEM (mmol L^{-1})

	Na^+	K^+	Mg^{2+}	Ca^{2+}	Cl^-	HCO_3^-	HPO_4^{2-}	SO_4^{2-}
SBF	142.0	5.0	1.5	2.5	105.0	27.0	1.0	0.5
DMEM	154.5	5.4	0.8	1.8	118.5	44.0	0.9	0.8

2.3. In Vitro Assays. A small volume (∼25 mm^3) of the glass scaffolds was cut and immersed at 37 °C for 15 min, 30 min, 1 h, 6 h, 12 h, 1 day, and 2 days in 45 mL of a standard Dulbecco's modified Eagle medium (DMEM, Biochrom AG, Germany). The surface area of the sample/volume of the solution ratio used was 50 cm^{-1}. DMEM contains inorganic salts, glucose, amino acids, and vitamins and is widely used for cell culture (Table 1). The inorganic salts concentrations in DMEM are almost equal to simulated body fluids (SBF). Because proteins are present in DMEM, lower rates for the materials dissolution and a subsequent delay in surface layer formation are to be expected when compared to soaking in SBF because SBF is strictly an electrolyte solution. Indeed proteins from DMEM are charged species that can be attracted by the negative glass surface and coat it with a film. However, DMEM grants better testing conditions to simulate a biological environment. Moreover, it is commonly used as an osteoblast culture media; thus, we decided to use it in the present study in view of confronting with further biological results.

After interaction, the samples were removed from the fluid, air-dried, and embedded in resin (AGAR, Essex, England). Before characterization, the glass scaffolds were cut into thin sections of 500 μm nominal thickness using a low speed diamond saw. Then, the sections were placed on a mylar film with a hole of 3 mm in the center. This preparation protocol permits to obtain smooth sections, which are needed to perform micro ion beam analysis. Moreover, sections done in the core of the glass foams allows detailed examination at the pore surface.

2.4. Micro-PIXE-RBS Analysis. Analyses of the biomaterial/biological fluids interface were carried out using nuclear microprobes at CENBG (Centre d'Études Nucléaires de Bordeaux-Gradignan, France). The experimental characteristics of the CENBG microbeamline have been published previously (16). For PIXE-RBS analyses, we chose proton scanning microbeam of 1.5 MeV energy and 60 pA in intensity. The beam diameter was nearly 1 μm. An 80 mm^2 Si(Li) detector was used for X-ray detection, oriented at 135° with respect to the incident beam axis, and equipped with a beryllium window 12 μm thick. PIXE spectra are treated with the software package GUPIX (17). The quantification of PIXE spectra is generally done by using internal standards defined in GUPIX, but an external standard can be used specially when a filter is placed in front of the Si(Li) detector. This method allows a chemical analysis with an excellent sensitivity of several ppm thanks to the very good signal to background ratio. Compared to other techniques, like SEM/EDS, PIXE method allows an improvement of the sensitivity up to 3 orders of magnitude. This is a great advantage to study the distribution and the role of relevant bone trace elements (Sr, Mg, Zn) which can induce specific cellular

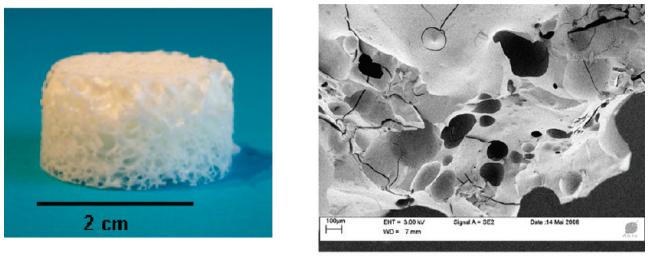

a b

FIGURE 1. (a) Numerical photograph of a SiO_2−CaO glass scaffold after synthesis. (b) SEM image of the same sample.

responses or can modify the bioactive process (18, 19). Relating to RBS, a silicon particle detector placed at 135° from the incident beam axis provided us with the number of protons that interacted with the sample. Data were treated with the SIMNRA code (20).

3. RESULTS AND DISCUSSION

3.1. Morphology and Porosity Analyses. The skeleton density of the sample is found to be 2.384 ± 0.007 g cm^{-3} in good agreement with such glass composition. Apparent density was 0.24 ± 0.01 g cm^{-3} corresponding to a total porous fraction of 90%. Such ultraporous materials should maximize cell/material interaction in cell engineering applications (9). The obtained cylindrical foams exhibit pores on multiple length scale as shown in Figure 1a and b. The SEM micrograph shows the pores with a diameter under 500 μm, which are present at the surface of pores with a diameter higher than 500 μm. The interconnected nature of macropores recalls the structure of trabecular bone (Figure 1a).

The BET surface area, the average and modal pore diameters, and the total pore volume have been calculated. The surface area is of the order of 166 m^2 g^{-1}; the BJH average pore diameter is 18 nm, and the total pore volume is 0.764 cm^3 g^{-1}. The mesopores are mainly responsible for the specific surface area and should control the kinetics of physicochemical reactions occurring at the glass surface, whereas macropores provide the ideal space for cell adhesion, differentiation, and tissue mineralization.

3.2. Chemical Maps of the Scaffolds. Elemental maps for each immersion time in DMEM were recorded. Figures 2 and 3 present the elemental distribution in a SiO_2−CaO scaffold before interaction with biological fluids. These chemical maps represent the number of characteristic X-rays detected. This number increase from the bottom to the top of the scale. Concerning trace elements, low quantities of X-rays coming from the background can be observed on the maps because X-rays intensities generated by trace elements are not high enough. Silicon and calcium distributions are homogeneous in the material as usually observed for sol−gel glasses. We can observe porosities of different sizes, ranging from 10 up to 800 μm. Macropores are created by the foaming process during samples preparation. The size of these pores is very promising for tissue engineering applications to guide the cell growth and to allow the synthesis of extracellular matrix in the human body. Glass scaffolds exhibit two kinds of porosity at the mesoporous and macroporous scale. PIXE/RBS resolution appears to be well adapted for the study of macropores reactivity on a local scale.

After 30 min of immersion in biological fluids, chemical maps demonstrate the formation of a Ca rich layer (which is about 5 μm thick) at the pore surface of the glass scaffold (Figure 4). Figure 5 shows the glass scaffold after 2 days of immersion. We can observe the glass at the center and two pores (one on the left and the second in the right top corner). The core of the glass mainly contains silica, whereas the surface layers of the two pores are now composed of Ca and P (Figure 5). The thickness of this layer has increased up to 10 μm. At this delay, pores with a diameter higher than 30 μm are essentially empty because the thickness of the Ca−P layer is on the order of 10 μm, and the medium must be removed before embedding in resin.

3.3. Concentrations Measurements in Glass Scaffolds and at Their Surface. Depending on the elements distributions, chemical maps were divided into various regions of interest using the SUPAVISIO analysis software. Thin masks of measurement were created (i.e., focusing on the X-ray spectra of some user-defined regions of interest), allowing the calculation of elemental concentrations in these areas. Depending on the region, masks from 3×3 up to 20×20 μm^2 were defined. Two series of masks were performed: (i) in the inner part of the scaffolds that

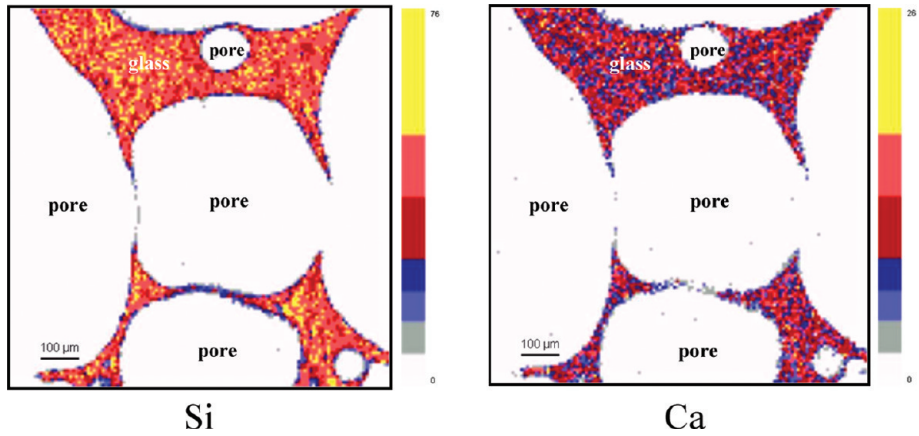

FIGURE 2. Elemental maps of a SiO_2−CaO glass scaffold before interaction with biological fluids (1000 × 1000 μm^2).

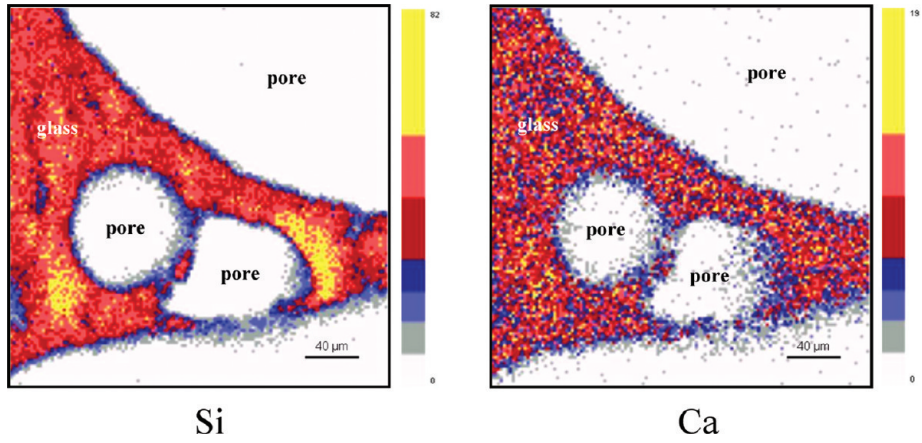

FIGURE 3. Elemental maps of a SiO_2−CaO glass scaffold before interaction with biological fluids (280 × 280 μm^2).

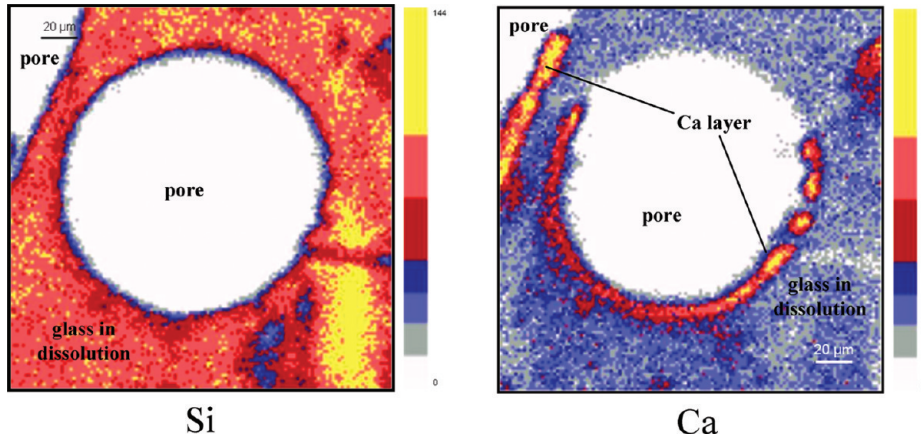

FIGURE 4. Elemental maps of a SiO_2−CaO glass scaffold after 30 min of interaction with biological fluids (205 × 205 μm^2).

were not directly exposed to biological fluids and (ii) at their surface (for short delays of immersion in biological fluids) or in the peripheral layer when detected. With this methodology, the evolutions of elemental concentrations in the glass scaffold and at the glass periphery can be observed and are presented in Tables 2 and 3, respectively. The results correspond to the average concentrations calculated in several analyzed parts. These regions of interest were defined over various samples in order to be ensured of measurements reproducibility. Each point represents an average of at least 5 measurements. Errors on elemental concentrations were determined by calculating the root-mean-square of errors related to each measure. They mainly depend on 4 parameters: the statistical error associated to the determination of the elemental peak area, the fit error, the error because of the overlapping peak areas and the errors related to instrumental factors (mainly due to the determination of the electric charge deposited on the samples and due to the irradiation damages).

The elemental concentrations measured in the material reveal changes in the material composition (Table 2). During immersion in DMEM, we observe an increase of Si concentration from 35.18% to 42.83% after 2 days and a decrease of Ca concentrations from 14.91% to 1.51% after 2 days. In fact, the relative increase in Si concentration is correlated with the decrease in Ca concentration. In the inner part of the glass foam, Si and Ca concentrations evolve in an opposite way because Si and Ca oxides content represent nearly 100% of the glass. Fluctuations in Si and Ca concentrations during the first 2 days are explained by the deep structural changes occurring in the glass network. The first step of the bioactivity process is the dealkalinization by rapid exchange of Ca^{2+} cations with H^+ from solution. This step is accelerated compared to dense glass (21) because of increased surface of interaction due to the mesopores. Hence, Ca concentration in the material decreased rapidly during the first 12 h of exposure to the biological medium. This reaction is immediately followed by a breakdown of the silica network enduring dissolution, forming silanol bonds at the glass interface (2nd step) that repolymerize to form a hydrated, high surface-area, silica-rich layer (3rd step). The breakdown of the glass network occurs rapidly and the release in calcium is higher than the release in silicon.

Elemental concentrations measured at the surface of scaffolds confirm physicochemical reactions occurring at the glass foams periphery (Table 3). After 15 min of immersion, the glass surface is depleted in Si and enriched in Ca. This Ca-rich layer results from the diffusion of the released Ca from the inner of the glass scaffold to its surface. It is worth noting that after 1 h of immersion, traces of phosphorus, coming from the biological medium, are already incorporated in this layer. The ionic exchanges and the physicochemical reactions then continue to feed the growth of this layer which contains P and Ca. We also observe that after 2

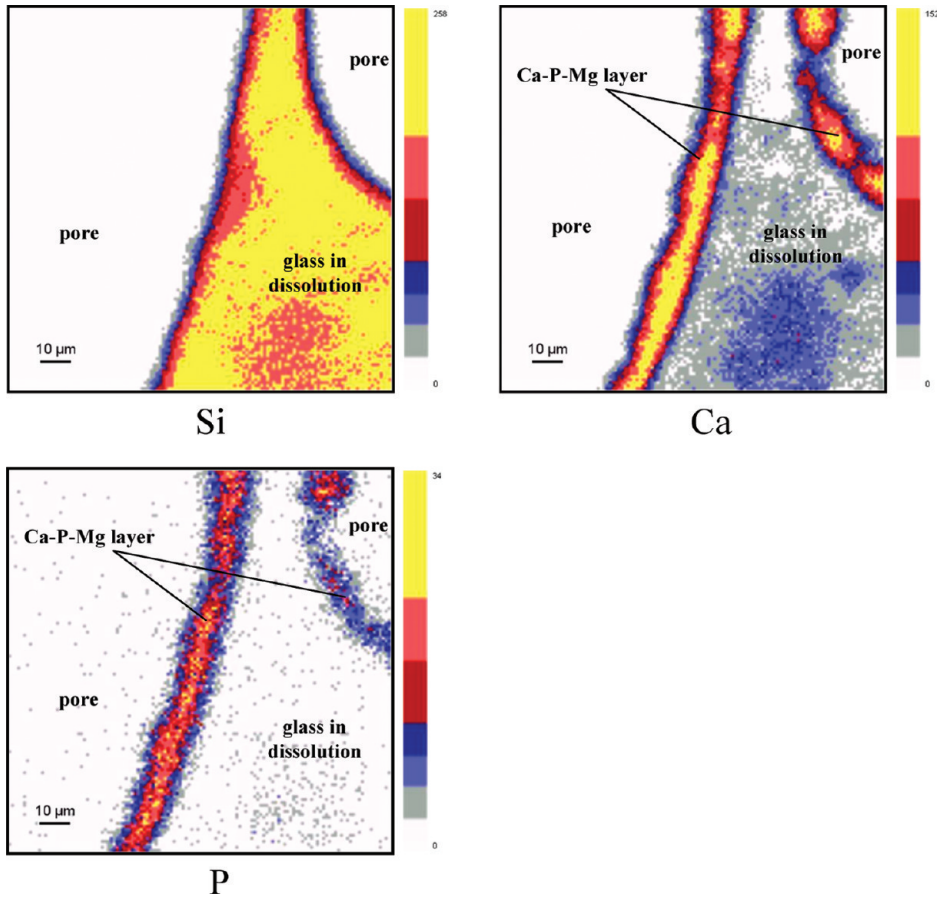

FIGURE 5. Elemental maps of a SiO_2−CaO glass scaffold after 2 days of interaction with biological fluids (125 × 125 μm^2).

Table 2. Evolution of Si and Ca Concentrations (wt %) Calculated in the Inner Regions of a SiO_2−CaO Glass Scaffold with Time of Exposure to Biological Fluids

	0 min	15 min	30 min	1 h	6 h	12 h	1 d	2 d
Si	35.18 ± 0.79	36.12 ± 0.85	36.14 ± 0.94	37.26 ± 0.94	37.90 ± 0.98	42.23 ± 0.94	42.69 ± 1.12	42.83 ± 0.96
Ca	14.91 ± 0.47	13.54 ± 0.50	13.23 ± 0.64	11.54 ± 0.56	11.62 ± 0.61	3.15 ± 0.20	1.04 ± 0.26	1.51 ± 0.10

Table 3. Evolution of Si, Ca, P, and Mg Concentrations (wt %) Calculated at the Pore Surface of a SiO_2−CaO Glass Scaffold with Time of Exposure to Biological Fluids

	0 min	15 min	30 min	1 h	6 h	12 h	1 d	2 d
Si	35.18 ± 0.79	14.80 ± 0.75	12.78 ± 0.79	11.32 ± 0.41	5.92 ± 0.47	5.19 ± 0.23	3.99 ± 0.23	2.49 ± 0.20
Ca	14.91 ± 0.47	42.97 ± 1.89	45.77 ± 1.70	46.47 ± 1.26	49.23 ± 1.83	56.18 ± 1.33	53.70 ± 1.41	47.26 ± 1.26
P				0.37 ± 0.11	0.38 ± 0.15	0.39 ± 0.10	4.03 ± 0.95	5.80 ± 0.29
Mg								0.42 ± 0.05

days of immersion traces of Mg are taken from biological fluids and incorporated into the layer. Traces of Si from the initial glassy network still remain. Formation of this Ca−P−Mg layer represents the bioactivity process occurring at the glass scaffolds surface. After 2 days, calcium and phosphorus concentrations in the layer are 47.26% and 5.80%, respectively. These concentrations correspond to a high Ca/P atomic ratio compared to the 1.67 value of $Ca_{10}(PO_4)_6(OH)_2$ stoichiometric hydroxyapatite (HA) of adult-human calcified bone. Quantities of phosphorus provided by the biological medium are not enough to permit the development and the formation of the bone-like apatite layer in that ultraporous materials at a short time period. In the case of ultraporous materials like glass foams in the binary system, it would be interesting to perform interactions in dynamic conditions which are closer to in vivo conditions. This could permit to demonstrate biomineralization process usually observed for many P-free glasses under another form (powders, monoliths) (22, 23). Nevertheless, the phosphorus-free glass scaffold is a good candidate to observe the modification of the glass surface in biological conditions. Because of the absence of phosphorus in the starting glass composition, it has been possible for the first time to directly follow in situ the biomineralization in glass foams with a spatial resolution lower than the pore size. The absence of phosphorus does not affect the experimental investigation but the apparition of low concentrations of P in the first steps of biomineralisation is easier to be detected and demonstrated.

Thanks to PIXE associated to RBS and its inherent sensitivity, it is possible to specify the role of trace elements in physicochemical reactions occurring at the periphery of bioactive scaffolds. Moreover, with its spatial resolution, quantitative chemical mapping for nearly all elements are available giving access to a direct monitoring of chemical reactions taking place. A further very important advantage is that PIXE can be used as a microbeam or nanobeam technique, which permits elemental mapping with a good spatial resolution and to quantify locally elemental concentrations on define regions of interest. However, the nanoscale structure is still out of reach with these techniques. To complete these measurements, it is important to mention that recent atomistic simulations of bioactive glass surfaces and interfaces can provide realistic information at the nanometer level, even though on a much smaller sample, about these systems (24, 25).

4. CONCLUSION

Micro-PIXE-RBS methodology allowed specifying the role of major and trace elements in physicochemical reactions occurring at the surface of pores in SiO_2−CaO glass scaffold. In contact with body fluids, bioactive glasses induce a specific biological response at their pore surface. The initial SiO_2−CaO glass network is quickly enduring dissolution with a high release of calcium. Then, following the different stages of the bioactivity process, a calcium phosphate-rich layer formation and evolution of the glass network are highlighted. Magnesium is proved to be blended into the phosphocalcic layer: this is of major importance since magnesium can play an important role during spontaneous formation of in vivo calcium phosphates and bone bonding (26). The specific preparation protocol developed permits the characterization at the micrometer scale of physicochemical reactions occurring at the surface of glass foams.

We have demonstrated that quantities of phosphorus provided by the biological medium played a key role in the development and the formation of the bone-like apatite layer. P_2O_5-free glass scaffolds do not lead to a rapid formation of an apatite layer. Phosphorus-based glass scaffolds should improve formation of this layer and it might permit, in vivo, an improved bonding ability with host tissues. Studies on scaffolds in the SiO_2−CaO−P_2O_5 system are now being performed to confirm this point.

Acknowledgment. Ł.J. would like to thank the Foundation for Polish Science (START Programme for Young Scientists) for their support and Conseil Régional d'Auvergne under project MABIO for financial support.

REFERENCES AND NOTES

(1) Lao, J.; Nedelec, J.-M.; Jallot, E. *J. Mater. Chem.* **2009**, *19*, 2940.
(2) Hench, L. L.; Splinter, R.; Allen, W.; Greenlee, T. *J. Biomed. Mater. Res.* **1971**, *2*, 117.
(3) Josset, Y.; Nasrallah, F.; Jallot, E.; Lorenzato, M.; Duffour-Mallet, O.; Balossier, G.; Laurent-Maquin, D. *J. Biomed. Mater. Res. A* **2003**, *67*, 1205.
(4) Padilla, S.; Román, J.; Carenas, A.; Vallet-Regí, M. *Biomaterials* **2005**, *26*, 475.
(5) Jallot, E.; Benhayoune, H.; Kilian, L.; Irigaray, J.-L.; Barbotteau, Y.; Balossier, G.; Bonhomme, P. *J. Colloid Interface Sci.* **2001**, *233*, 83.
(6) Tsigkou, O.; Jones, J. R.; Polak, J. M.; Stevens, M. M. *Biomaterials* **2009**, *30*, 3542.
(7) Xynos, I. D.; Edgar, A. J.; Buttery, L. D. K.; Hench, L. L.; Polak, J. M. *Biochem. Biophys. Res. Commun.* **2000**, *276*, 461.
(8) Laquerrière, P.; Jallot, E.; Kilian, L.; Benhayoune, H.; Balossier, G. *J. Biomed. Mater. Res. A* **2003**, *65*, 441.
(9) Jones, J. R.; Ehrenfried, L. M.; Hench, L. L. *Biomaterials* **2006**, *27*, 964.
(10) Hench, L. L.; West, J. K. *Chem. Rev.* **1990**, *90*, 33.
(11) Chen, Q. Z.; Thompson, I. D.; Boccaccini, A. R. *Biomaterials* **2006**, *27*, 2414.
(12) Lao, J.; Nedelec, J.-M.; Jallot, E. *J. Phys. Chem. C* **2008**, *112*, 9418.
(13) Jones, J. R.; Hench, L. L. *J. Biomed. Mater. Res., Part B* **2004**, *68*, 36.
(14) Jones, J. R.; Hench, L. L. *J. Mater. Sci.* **2003**, *38*, 3783.
(15) Sepulveda, P.; Jones, J. R.; Hench, L. L. *J. Biomed. Mater. Res.* **2002**, *59*, 340.
(16) Incerti, S.; Zhang, Q.; Andersson, F.; Moretto, Ph.; Grime, G. W.; Merchant, M. J.; Nguyen, D. T.; Habchi, C.; Pouthier, T.; Seznec, H. *Nucl. Instrum. Methods B* **2007**, *260*, 20.
(17) Maxwell, J. A.; Teesdale, W. J.; Campbell, J. L. *Nucl. Instrum. Methods B* **1995**, *95*, 407.
(18) Soulié, J.; Nedelec, J. M.; Jallot, E. *Phys. Chem. Chem. Phys.* **2009**, *44*, 10473.
(19) Lao, J.; Jallot, E.; Nedelec, J.-M. *Chem. Mater.* **2008**, *20*, 4969.
(20) Mayer, M. *Nucl. Instrum. Methods B* **2002**, *194*, 177.
(21) Lao, J.; Nedelec, J.-M.; Moretto, Ph.; Jallot, E. *Nucl. Instrum. Methods B* **2006**, *245*, 511.
(22) Salinas, A. J.; Vallet-Regi, M.; Izquierdo-Barba, I. *J. Sol−Gel Sci. Technol.* **2001**, *21*, 13.
(23) Lao, J.; Nedelec, J.-M.; Moretto, Ph.; Jallot, E. *Surf. Interface Anal.* **2008**, *40*, 162.
(24) Tilocca, A.; Cormack, A. N. *Langmuir* **2010**, *26*, 545.
(25) Tilocca, A. *Phys. Rev. B* **2007**, *76*, 224202.
(26) Jallot, E. *Appl. Surf. Sci.* **2003**, *211*, 89.

AM1002316